Deficiency of PARP-1 and PARP-2 in the mouse uterus results in decidualization failure and pregnancy loss

Andrew M. Kelleher[a,b], Rohit Setlem[a,b], Françoise Dantzer[c], Francesco J. DeMayo[d], John P. Lydon[e], and W. Lee Kraus[a,b,1]

[a]Laboratory of Signaling and Gene Regulation, Cecil H. and Ida Green Center for Reproductive Biology Sciences, University of Texas Southwestern Medical Center, Dallas, TX 75390; [b]Division of Basic Research, Department of Obstetrics and Gynecology, University of Texas Southwestern Medical Center, Dallas, TX 75390; [c]Poly(ADP-ribosyl)ation and Genome Integrity, Institut du Médicament de Strasbourg, UMR 7242-Biotechnologie et Signalisation Cellulaire, CNRS/Université de Strasbourg, 67412 Illkirch, France; [d]Reproductive and Developmental Biology Laboratory, National Institute of Environmental Health Sciences, Durham, NC 27709; and [e]Department of Molecular and Cellular Biology, Baylor College of Medicine, Houston, TX 77030

Edited by Janet Rossant, Gairdner Foundation, Toronto, ON, Canada, and approved August 23, 2021 (received for review May 18, 2021)

Miscarriage is a common complication of pregnancy for which there are few clinical interventions. Deficiency in endometrial stromal cell decidualization is considered a major contributing factor to pregnancy loss; however, our understanding of the underlying mechanisms of decidual deficiency are incomplete. ADP ribosylation by PARP-1 and PARP-2 has been linked to physiological processes essential to successful pregnancy outcomes. Here, we report that the catalytic inhibition or genetic ablation of PARP-1 and PARP-2 in the uterus lead to pregnancy loss in mice. Notably, the absence of PARP-1 and PARP-2 resulted in increased p53 signaling and an increased population of senescent decidual cells. Molecular and histological analysis revealed that embryo attachment and the removal of the luminal epithelium are not altered in uterine *Parp1*, *Parp2* knockout mice, but subsequent decidualization failure results in pregnancy loss. These findings provide evidence for a previously unknown function of PARP-1 and PARP-2 in mediating decidualization for successful pregnancy establishment.

pregnancy | uterus | PARP-1 | PARP-2 | ADP-ribosylation

Pregnancy loss (miscarriage) is a common complication in human pregnancy, and defects arising during early implantation are significant factors contributing to adverse pregnancy outcomes (1, 2). Although fetal chromosomal abnormalities underlie the majority of sporadic miscarriages, the incidence of chromosomal abnormality decreases in the case of recurrent pregnancy loss, suggesting the importance of the uterine environment (3, 4). Currently, few clinical interventions are available for recurrent pregnancy loss, warranting the need to identify and explore understudied mechanisms involved in the successful establishment of pregnancy.

Perturbations in early pregnancy events, such as embryo implantation and stromal cell decidualization, can lead to adverse ripple effects that compromise pregnancy outcomes (2). Successful embryo attachment and subsequent development into the underlying endometrium rely on the coordinated regulation of decidualization. Decidualization is the postovulatory process of endometrial remodeling in preparation for pregnancy (5). It is characterized by the coordinated proliferation and differentiation of endometrial stromal cells into large epithelioid decidual cells, the secretory transformation of the uterine glands, and vascular remodeling (5–7). Several recent studies have found that defective stromal cell decidualization can result in pregnancy complications, such as preeclampsia, pregnancy loss, and miscarriage, yet the underlying molecular mechanisms remain unclear (2, 8–10).

ADP ribosylation (ADPRylation), the covalent attachment of a single ADP ribose (ADPR) or polymers of ADPR units on target proteins, is catalyzed by the poly(ADPR) polymerase (PARP) family of enzymes (11, 12). PARPs 1 and 2, the predominant nuclear PARPs, catalyze the polymerization of linear or branched chains of ADPR, called poly(ADPR) or PAR (11, 13). Initial studies of nuclear PARPs focused on DNA repair, whereas more recent studies have shifted the focus to the regulation of chromatin structure and gene expression (13). Of note, PARPs 1 and 2 bind to chromatin at crucial regulatory regions across the genome, including promoters and enhancers (14–17), in which they can regulate gene expression through chromatin-dependent mechanisms (18, 19). Furthermore, a growing body of work has shown that transcription factors and coregulators are regulated by site-specific ADPRylation (20–23).

The roles of PARP-1 and PARP-2 have not been explored extensively in the context of female reproductive biology, despite their essential functions in related physiological processes that govern pregnancy success, such as metabolism, inflammation, immunity, stress responses, and hormonal signaling (11, 13). Individual knockouts of *Parp1* or *Parp2* in mice are viable and have been widely studied in the context of DNA damage and inflammatory responses (13). In contrast, knockout of both *Parp1* and *Parp2* results in embryonic lethality at around the time of gastrulation (24, 25). The lack of viability precludes the use of double null animals in the study of potential redundant roles of PARP-1 and PARP-2 in female reproductive biology. Here, we conducted a series of studies with *Parp1*;*Parp2* double conditional knockout (*P1P2* cKO) mice to understand the role of PARPs 1 and 2 and ADPRylation in the context of uterine and pregnancy biology. Our studies provide evidence that PARP-1 and PARP-2 and, by inference, their ADPRylated substrate proteins are critical to

Significance

This study identifies an unknown role for PARP-1 and PARP-2 in mediating pregnancy success. Utilizing a combination of mouse genetic models, pharmacological inhibitors, and histological and transcriptomic analysis, we identified roles for PARPs and ADP ribosylation (ADPRylation) during the establishment and maintenance of pregnancy. We show that the absence of PARP-1 and PARP-2 augments the DNA damage response during early pregnancy, presumably by ADPRylating substrate proteins, culminating in aberrant decidualization and ultimately pregnancy failure. These findings could be leveraged to develop contraceptives or as biomarkers of uterine receptivity and stromal cell decidualization.

Author contributions: A.M.K. and W.L.K. designed research; A.M.K. performed research; F.D., F.J.D., and J.P.L. contributed mouse genetic models; A.M.K., R.S., and W.L.K. analyzed data; A.M.K. and W.L.K. wrote the paper; and W.L.K. obtained research support and provided overall project direction.

Competing interest statement: W.L.K. is a founder, consultant, and Scientific Advisory Board member for Ribon Therapeutics, Inc. and ARase Therapeutics, Inc. He is also co-holder of US Patent 9,599,606 covering the ADP-ribose detection reagent used herein, which has been licensed to and is sold by EMD Millipore.

This article is a PNAS Direct Submission.

Published under the PNAS license.

[1]To whom correspondence may be addressed. Email: lee.kraus@utsouthwestern.edu.

This article contains supporting information online at https://www.pnas.org/lookup/suppl/doi:10.1073/pnas.2109252118/-/DCSupplemental.

Published September 27, 2021.

Downloaded at Palestinian Territory, occupied on December 21, 2021

www.manaraa.com

stromal cell decidualization and the successful establishment of pregnancy.

Results

Inhibition of PARP-1 and PARP-2 Catalytic Activity Results in Pregnancy Loss. Despite their essential roles in related physiological processes that govern pregnancy success, the roles of PARP-1 and PARP-2 have not been studied extensively in the context of pregnancy. To address this, we first profiled the levels of ADPRylation throughout gestation. We observed significant alterations in the levels of ADPRylation from early pregnancy to late pregnancy. Of note, the highest levels of ADPRylation were during the first half of pregnancy, followed by a dramatic decrease at gestational day 12 (GD 12) until term pregnancy (Fig. 1 *A* and *B*). We used Niraparib (Nir), a US Food and Drug Administration (FDA)–approved inhibitor of PARP-1 and PARP-2 catalytic activity, to determine the impact of nuclear PARP-mediated ADPRylation on pregnancy success. Pregnant female mice were treated with Nir (25 mg/kg) on GD 3 and GD 4 (Fig. 1*C*), which efficiently inhibited ADPRylation in the implantation sites of pregnant mice (Fig. 1*D*). Nir-treated females produced no offspring, whereas vehicle-treated female mice produced litters of normal size (Fig. 1*E*).

To determine the stage of pregnancy at which inhibition of PARP-1 and PARP-2 resulted in pregnancy loss, mice were treated with either vehicle or Nir, and implantation was examined in uteri collected on GDs 6, 8, and 12. Implantation sites were observed in vehicle- and Nir-treated animals independent of GD (Fig. 1 *F*, *H*, and *J*). Likewise, there was no difference in implantation site number between control and treated animals (Fig. 1 *G*, *I*, and *K*). In contrast, implantation site diameter was reduced on GD 6 and 8, with clearly resorbing implantation sites observable on GD 12 (Fig. 1 *G*, *I*, and *K*). Indeed, the dissection of GD 12 implantation sites revealed no discernable placenta or embryo in Nir-treated females (Fig. 1*L*). Taken together, these data reveal a critical role for PARP-1 and PARP-2 catalytic activity in regulating successful pregnancy.

Genetic Ablation of *Parp1* and *Parp2* in the Uterus Causes Infertility or Severe Subfertility. To circumvent the embryonic lethality of global *Parp1* and *Parp2* knockout (24, 25) and the systemic inhibition using pharmacological inhibitors, we used conditional knockout (cKO) of *Parp1* and *Parp2* to study their role in adult uterine function. PARP-1 and PARP-2 are expressed in most organs and cell types and, likewise, are expressed in all major cell types of the endometrium during early pregnancy. Immunofluorescent staining analysis revealed nuclear staining in the luminal epithelium, glandular epithelium, and stroma, independent of the GD (*SI Appendix*, Fig. S1). *Parp1* and *Parp2* floxed mice ($Parp1^{f/f}$;$Parp2^{f/f}$) were crossed to mice harboring the progesterone receptor (PR) gene promoter (*Pgr*)-Cre driver, which recombines alleles in the *Pgr*-expressing cells in reproductive tissues, including epithelial and stromal compartments of the uterus (26). Compared to controls, *Parp1* and *Parp2* messenger RNA (mRNA) levels, and PARP-1 and PARP-2 protein levels were significantly reduced in the uteri but not the ovaries of GD 4 Pgr^{Cre};$Parp1^{f/f}$;$Parp2^{f/f}$ (*P1P2* cKO) mice (Fig. 2 *A*–*C*). Fertility tests of female wild-type control ($Parp1^{f/f}$;$Parp2^{f/f}$), individual knockouts of *Parp1* (Pgr^{Cre};$Parp1^{f/f}$;$Parp2^{wt/wt}$) and *Parp2* (Pgr^{Cre};$Parp1^{f/f}$;$Parp2^{wt/wt}$), and *P1P2* cKO mice over 6 mo revealed that individual cKOs for *Parp1* and *Parp2* exhibited normal fertility and fecundity (6.0 and 6.4 pups/litter, respectively). In contrast, the *P1P2* cKO mice were severely subfertile or infertile compared to controls (only three *P1P2* cKO females produced litters of two or less pups) (Fig. 2 *D*–*G*).

Reduction in the size and number of implantation sites, as well as abnormal implantation site histology, was evident on GD 10 in *P1P2* cKO mice, compared to control females. Of note, only half of the *P1P2* cKO mice had visual implantation sites at necropsy on GD 10 (*SI Appendix*, Fig. S2 *A*–*C*). Western blots and immunofluorescence analyses demonstrated no notable differences between genotypes in the uterine expression or localization of estrogen receptor alpha or PR on GD 4 (Fig. 2*C* and *SI Appendix*, Fig. S3 *D* and *E*). Importantly, female *P1P2* cKO mice showed normal ovulation, fertilization, ovarian morphology, and serum levels of circulating progesterone (*SI Appendix*, Fig. S3 *A*–*C*). These results suggest that the fertility defect observed in the *P1P2* cKO mice is primarily due to a defect in uterine function.

Genetic Ablation of *Parp1* and *Parp2* in the Uterus Does Not Disrupt Embryo Localization or Attachment. To determine the cause of infertility in *P1P2* cKO mice, we first investigated the impact of genetic ablation of *Parp1* and *Parp2* in the uterus on implantation and decidualization. On the afternoon of GD 4, blastocysts enter the uterus and become positioned in implantation crypts formed toward the antimesometrial (AM) region of the uterus prior to attachment (2, 8, 27). By the morning of GD 5, the attachment reaction has commenced, and the onset of stromal cell decidualization is evident. To assess blastocyst positioning and the initiation of implantation, we carefully examined implantation sites on the morning of GD 5. Hatched blastocysts were present within implantation crypts on the AM side of the uterus in both control and *P1P2* cKO mice at 0900 h on GD 5 (Fig. 3*A*), with no difference in the number of implantation sites (Fig. 3*B*).

The expression of prostaglandin-endoperoxide synthase 2 (PTGS2) commences on the morning of GD 5 in the decidualizing stromal directly adjacent to the implanting blastocyst and is one of the first histological markers of decidualization (28). Immunoblots of whole-uterine lysates from implantation sites showed comparable levels of PTGS2 (Fig. 3 *C* and *D*). In the same regard, implantation sites of both control and *P1P2* cKO mice contained PTGS2-positive stromal cells near the implanting embryo on GD5 (Fig. 3*E*). These results suggest that the initial embryo attachment and the onset of stromal cell decidualization proceed normally in *P1P2* cKO mice.

Genetic Ablation of *Parp1* and *Parp2* in the Uterus Compromises the Maternal Decidual Response. On the morning of GD 6, implantation sites from both control and *P1P2* cKO mice had normal numbers of implantation sites (Fig. 4 *A* and *B*). Histologically, the implantation sites of *P1P2* cKO appeared normal and were virtually indistinguishable from controls. The embryos were positioned centrally within implantation sites, luminal epithelial cells were absent from the lateral sites of the implantation chamber, and PTGS2-positive, decidualizing stromal cells were evident (*SI Appendix*, Fig. S4 *A* and *B*). However, implantation sites from *P1P2* cKO females were significantly smaller in comparison to control mice (Fig. 4 *A* and *B*). The staining pattern for Ki67 and cleaved caspase-3 was not altered in implantation sites on GD 6, suggesting that the differences cannot simply be explained because of reduced proliferative capacity or increased apoptosis around the implanting embryo (Fig. 4*C* and *SI Appendix*, Fig. S4 *B*–*D*).

Similar to GD 6, there was no difference in implantation site number on GD 8, and the diameter of implantation sites were greatly reduced (Fig. 4 *D* and *E*). Although embryos were present in GD 8 implantation sites of *P1P2* cKO mice, their morphology was much more variable, and the embryos were less developed than those of control mice (Fig. 4*F*). Delayed embryo development and embryo resorption are highlighted by the emergence of apoptotic cells adjacent to the developing embryo (Fig. 4*F*). Notably, the complete resorption of embryos and implantation sites were observed in three of the seven *P1P2* cKO mice on GD 10, while the remaining *P1P2* cKO mice had evident signs of active embryo resorption (*SI Appendix*, Fig. S2*A*).

We next examined the impact of genetic ablation of *Parp1* and *Parp2* in the uterus on decidualization, using a model of artificial decidualization. Control mice displayed robust deciduoma formation following intrauterine oil injection. In contrast, *P1P2* cKO mice exhibited a significant defect ($P < 0.01$) in the decidual response (*SI Appendix*, Fig. S5 *A* and *B*). This decidual

Downloaded at Palestinian Territory, occupied on December 21, 2021
www.manaraa.com

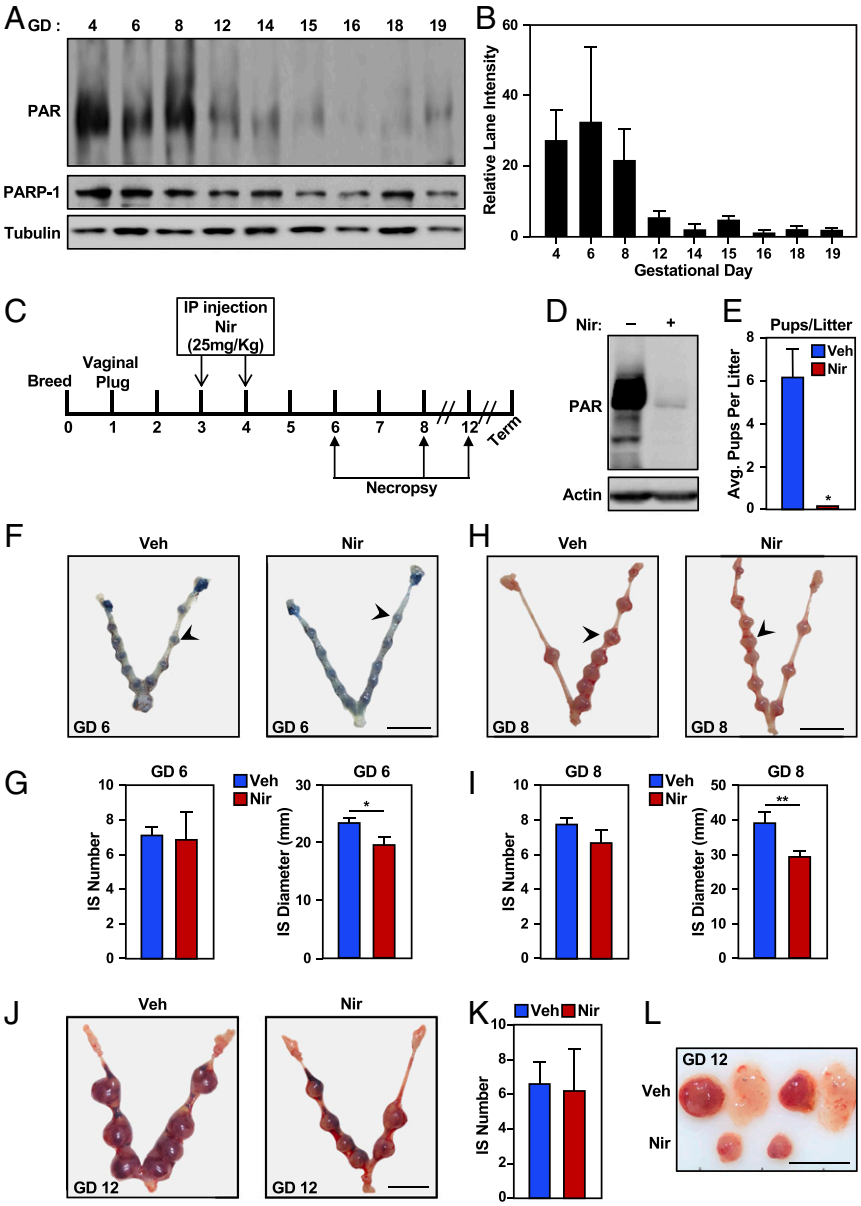

Fig. 1. Inhibition of PARP-1 and PARP-2 catalytic activity results in recurrent early pregnancy loss. (*A* and *B*) Western blot analysis (*A*) and quantification (*B*) of total PAR and PARP-1 at selected time points during murine pregnancy, as indicated. β-tubulin serves as a loading control ($n = 3$ per time point and mean ± SEM). (*C*) Experimental design for inhibition of PARP-1 and PARP-2 catalytic activity during murine pregnancy. Control mice received intraperitoneal (IP) injections of either vehicle (Veh) or Nir (25 mg/kg) on GDs 3 and 4 and were evaluated on GDs 6, 8, and 12 and at term ($n = 3$ mice per time point). (*D*) Western blot of total PAR on GD 8, following Nir treatment. (*E*) Pregnancy failure in mice that received injections of Nir ($n = 4$ and mean ± SEM). (*F* and *G*) Assessment of embryo implantation sites (*F*) and quantification of the number and diameter of implantation sites (*G*) in vehicle- and Nir-treated mice on GD 6 ($n = 4$, mean ± SEM). In *F*, black arrowheads point to individual implantation sites. (Scale Bars, 1 cm.) *$P < 0.05$ (Student's *t* test). (*H* and *I*) Assessment of embryo implantation sites (*H*) and quantification of the number and diameter of implantation sites (*I*) in vehicle- and Nir-treated mice on GD 8 ($n = 4$, mean ± SEM). In *H*, black arrowheads point to individual implantation sites. (Scale bars, 1 cm.) IS: implantation site. **$P < 0.01$ (Student's *t* test). (*J* and *K*) Gross morphology of uteri with embryo implantation sites (*J*) and quantification of implantation site number (*K*) in vehicle- and Nir-treated mice on GD 12 ($n = 4$ and mean ± SEM). (Scale bar, 1 cm.) (*L*) Contents of implantation site from dissection on GD 12. Scale bar, 1 cm.

defect was further confirmed by the quantification of the expression of mRNAs encoding decidualization markers, including prolactin family 8, subfamily a, member 2, bone morphogenetic protein 2, and homeobox A10 in the *P1P2* cKO mice (*SI Appendix*, Fig. S5*C*). Collectively, these data strongly suggest a decidual defect in the *P1P2* cKO mice.

PARP-1 and PARP-2 Influence the Uterine Transcriptome during Pregnancy. To further interrogate the underlying uterine defects resulting in pregnancy loss, we performed RNA sequencing (RNA-seq) on the whole uterus from GD 4 and implantation sites on GD 5 and GD 6 from control and *P1P2* cKO mice. Transcriptome profiling revealed differentially expressed genes (DEGs) on all three GDs (Fig. 5*A*). Of particular interest, a robust increase in the number of DEGs was observed as normal pregnancy progressed from GD 4 to GD 6. Based on statistical significance ($q < 0.05$) and a fold change greater than 1.5-fold in expression, only 103 genes differed between control and *P1P2* cKO mice on GD 4, whereas the number of DEGs increased to 1,341 and 3,790 on GD 5 and GD 6, respectively (Fig. 5*B*). A total

Downloaded at Palestinian Territory, occupied on December 21, 2021

www.manaraa.com

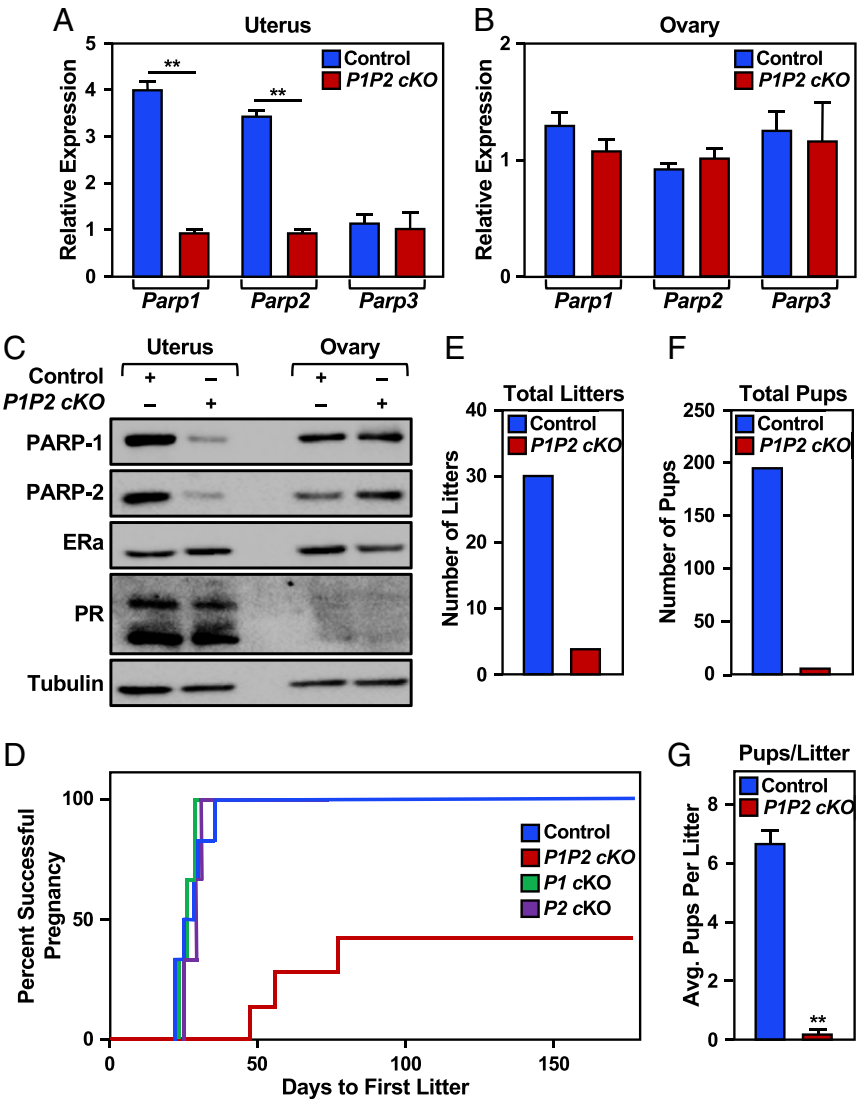

Fig. 2. Uterine deficiency of PARP-1 and PARP-2 results in severe subfertility. (*A* and *B*) RT-PCR of mRNA from the uterus (*A*) and ovary (*B*) ($n = 3$ per genotype and mean ± SEM). $^{**}P < 0.01$ (Student's *t* test). (*C*) Western blot of PARP-1, PARP-2, estrogen receptor alpha (ER-α), and PR in the uterus and ovary of *P1P2* cKO and control mice. (*D*) A 6-mo breeding study reveals uterine *P1P2* cKO mice are severely subfertile ($n = 7$). (*E*–*G*) Total litters (*E*), total pups (*F*), and average pups per litter (*G*) in control ($n = 6$) and *P1P2* cKO ($n = 7$) during the 6-mo breeding trial. $^{**}P < 0.01$ (Student's *t* test).

of 75 genes were differentially expressed on all 3 d of pregnancy profiled (Fig. 5*A*). Pathway analysis of those genes showed a significant enrichment of the p53 signaling pathway (*Bb3c*, *Ccng1*, *Cdkn1a*, *Gadd45g*, and *Sesn2*) (Dataset S1). Based on the large perturbation of the transcriptome on GD 6 from *Parp1* and *Parp2* knockout, compared to both GD 4 and GD 5, the rest of the analysis focused on GD 6 (during stromal cell decidualization).

Of the 3,790 DEGs on GD 6, 368 were up-regulated, and 3,422 were down-regulated. Gene ontology (GO) analysis of up-regulated genes revealed a significant enrichment of genes associated with signaling by p53, response to DNA damage, bone development, extracellular structure organization, and skeletal system development. In contrast, the down-regulated genes were enriched for genes involved in DNA replication, the regulation of mRNA metabolic processes, cell cycle phase transition, cell division, and the regulation of mitotic cell cycle (Fig. 5*C*). Of note, many of the DEGs have been implicated or are known to be involved in stromal cell decidualization (*Bmp7*, *Cdh1*, *Cebpb*, *Ptgs2*, *Ptx3*, and *Wnt4*) (29), thus supporting the conclusion that decidualization is compromised in the absence of PARP-1 and PARP-2 (Fig. 5*C*).

DNA Damage and p53 Expression Are Elevated in the Decidua of *P1P2* cKO Mice. The enrichment of signal transduction by p53 and response to DNA damage have been previously implicated in the regulation of decidualization (30–32). Thus, we determined if the transcriptional effects were reflected at the protein level. Our RNA-seq analysis did not demonstrate an increase in *Tp53* gene transcription in the implantation sites of *P1P2* cKO mice. However, Western blot analysis of GD 6 decidua from control and *P1P2* cKO mice confirmed an increase in the levels of p53, phospho-p53, and the phosphorylation of H2AX (gamma H2AX), a marker of DNA damage, in the decidua of *P1P2* cKO mice (Fig. 5 *D* and *E*). The increase in phospho-p53, which is a major posttranslational modification in the activation of p53 (33), was specific to the stromal cells and was not observed in epithelial cells or embryos within GD 6 implantation sites of either control or *P1P2* cKO mice (*SI Appendix*, Fig. S6*A*).

Downloaded at Palestinian Territory, occupied on December 21, 2021
www.manaraa.com

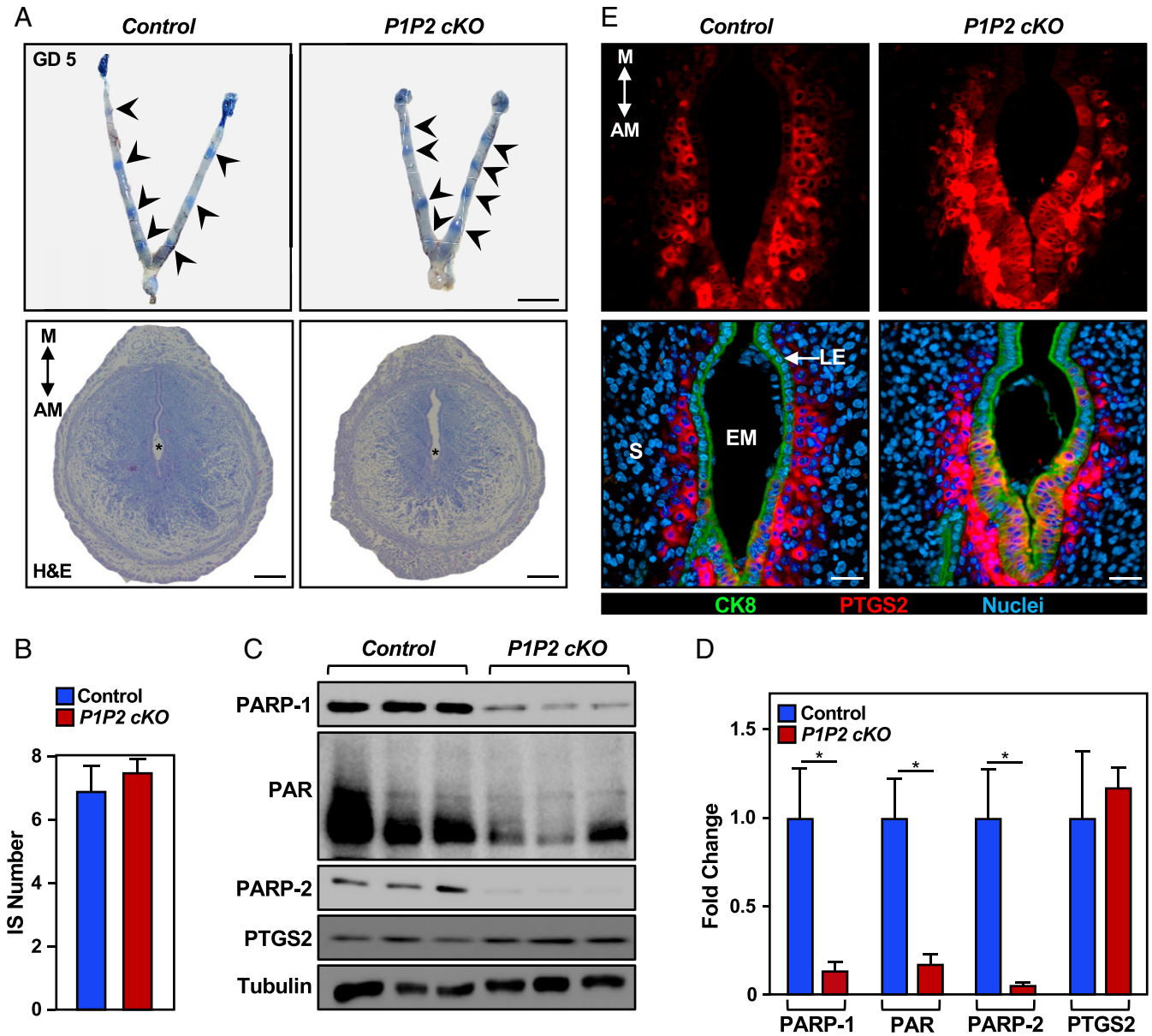

Fig. 3. The attachment reaction and onset of stromal cell decidualization proceed in the absence of uterine PARP-1 and PARP-2. (*A*) Gross morphology of uteri on GD 5 at 0900 h. Implantation site histology by hematoxylin and eosin (H&E) staining show embryos within implantation crypts on the AM pole of the uterus. Black arrowheads point to individual implantation sites, as assessed by Evans blue dye accumulation. (Scale bars, 1 cm; *Upper*.) (Scale bars, 200 μm; *Lower*.) M: mesometrial. (*B*) Quantification of number of implantation sites on GD 5. ($n = 4$ and mean ± SEM). IS: implantation site. (*C*) Western blot analysis of PARP-1, PAR, PARP-2, and PTGS2 from GD 6 implantation sites of control and *P1P2* cKO mice ($n = 3$ mice per time point). (*D*) Quantification of the results shown in *C* ($n = 3$ per genotype and mean ± SEM). *$P < 0.05$ (Student's *t* test). (*E*) Immunofluorescence analysis of PTGS2 and CK8 in implantation sites on GD 5. (Scale bars, 50 μm.) LE: luminal epithelium, S: stroma, and EM: embryo.

Since the ADPRylation of p53 is known to inhibit p53 interactions with its consensus DNA binding element, thus representing a means of regulating p53-dependent transcriptional activation (34–36), we examined the possibility that endogenous p53 is ADPRylated in GD 6 implantation sites. The immunoprecipitation of endogenous p53, followed by Western blot analysis, revealed that p53 is indeed ADPRylated (*SI Appendix*, Fig. S6*B*). One mechanism for the regulation of phosphorylation is via adjacent ADPRylation sites (22, 37, 38). In this regard, bioinformatic analysis using ADPredict, a computation tool used to predict the most probable sites of ADPRylation within a target protein (39), revealed that the top predicted sites of ADPRylation on p53 occur adjacent to the phosphorylation site on serine 15 (*SI Appendix*, Fig. S6*C*), suggesting possible ADPRylation–phosphorylation crosstalk. Taken together, these results suggest that the absence of PARP-1 and PARP-2 results in increased DNA damage, as well as enhanced phosphorylation and stabilization of p53, within the decidua.

A Senescence Signature Is Observed in the Decidua of *P1P2* cKO Mice. Classically, in response to DNA damage, p53 signaling can lead to apoptosis or cellular senescence (40). We observed an increase in the phosphorylation of H2AX but not a corresponding increase in cleaved caspase-3, a marker of apoptotic cell death, in the decidua of *P1P2* cKO mice on GD 6 (Fig. 6*A*). The inability to induce apoptosis in conditions of persistent DNA

Downloaded at Palestinian Territory, occupied on December 21, 2021

www.manaraa.com

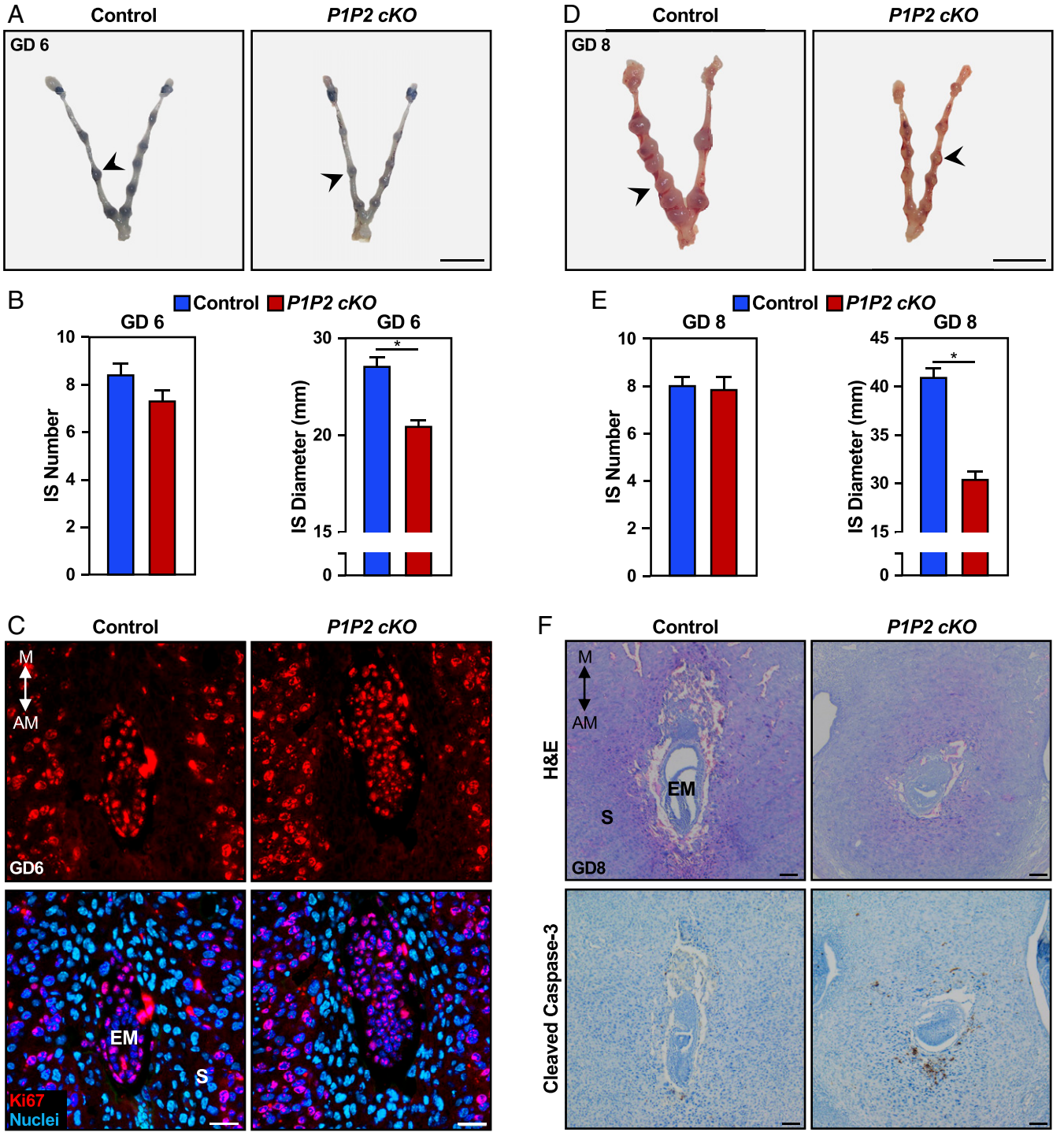

Fig. 4. Decreased implantation site size in pregnant PARP-1;PARP-2-deficient mice. (*A*) Gross morphology of uteri on GD 6 at 0900 h, as assessed by the accumulation of Evans blue dye. Black arrowheads point to an example implantation site ($n = 4$). (Scale bar, 1 cm.) (*B*) Quantification of the number and diameter of implantation sites on GD 6 ($n = 4$ and mean ± SEM). *$P < 0.05$ (Student's *t* test). IS: implantation site. (*C*) Immunofluorescence of Ki67 (cell proliferation marker) in implantation sites on GD 6 ($n = 3$). (Scale bars, 100 μm.) M: mesometrial, S: stroma, and EM: embryo. (*D*) Gross morphology of uteri on GD 8 at 0900 h. Black arrowheads point to an example implantation site ($n = 4$). (Scale bar, 1 cm.) (*E*) Quantification of the number and diameter of implantation sites on GD 8 ($n = 4$ and mean ± SEM). *$P < 0.05$ (Student's *t* test). (*F*) Implantation site histology by hematoxylin and eosin and immunolocalization of cleaved Caspase in GD 8 implantation sites ($n = 3$). (Scale bars, 100 μm.)

damage may lead to irreversible cell cycle arrest and senescence (41). In support of this hypothesis, we observed 1) an increase in *Cdkn1a* expression, a major target of p53 activity that links DNA damage to cell cycle arrest, and 2) reductions in the expression of *Lmnb1* and *Hmgb1*, biomarkers of senescence, in *P1P2* cKO mice (Fig. 6 *A* and *B*). The recent single-cell transcriptome analysis of human midluteal phase endometrium identified *SCARA5* and *DIO2* as marker genes for divergent decidual states of decidual cells and senescent decidual cells, respectively (42). Of note, we observed a decrease in *Scara5* and an increase in

Downloaded at Palestinian Territory, occupied on December 21, 2021
www.manaraa.com

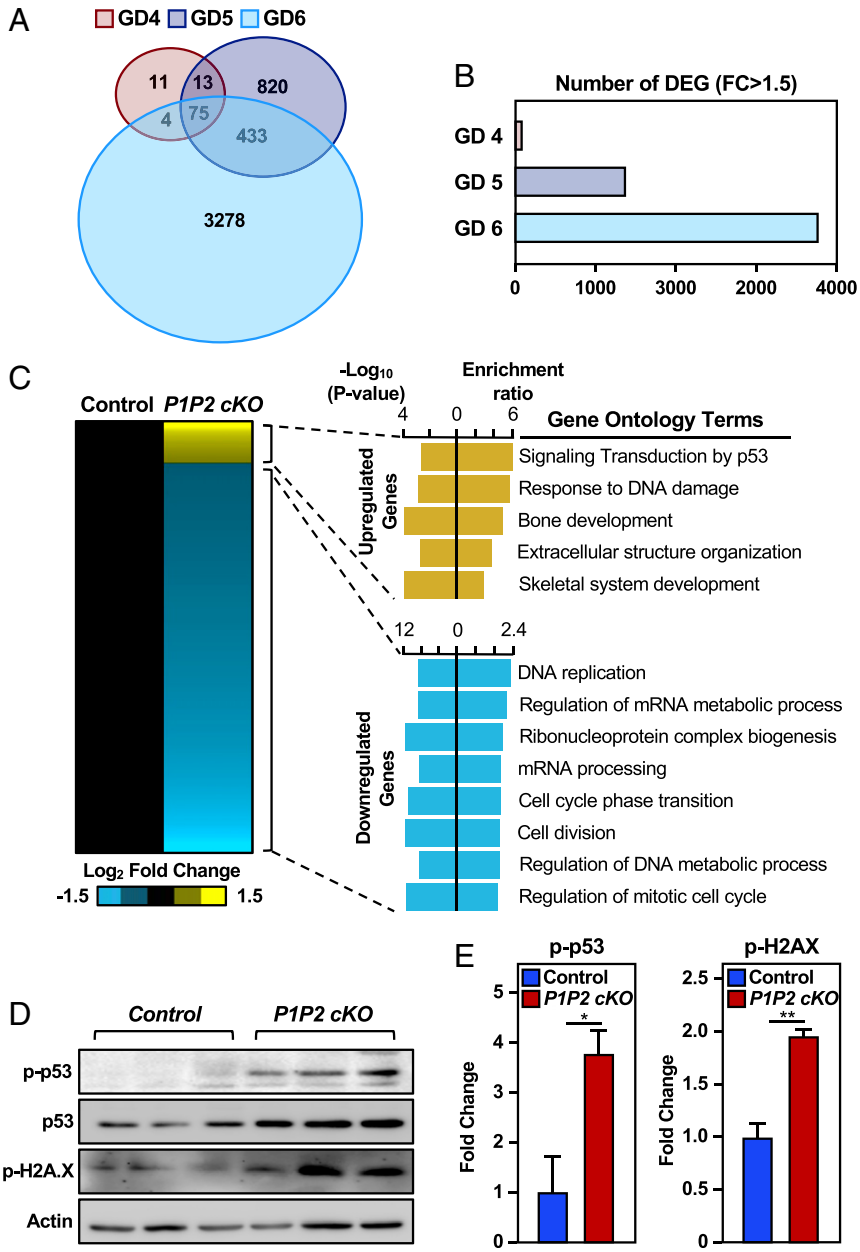

Fig. 5. The decidua of PARP-1;PARP-2 deficient mice displays increased DNA damage and p53 activation. (*A* and *B*) Venn diagram (*A*) and bar graph (*B*) depicting DEGs between *P1P2* cKO and control mice on GDs 4, 5, and 6 based on RNA-seq analysis. Fold change (FC) > 1.5. (*C*) Heatmap of DEGs and visualization of biological process GO terms associated with genes differentially expressed in control and *P1P2* cKO mice on GD 6. (*D*) Western blot analysis of pSer15-p53, p53, and p-H2A.X in GD6 implantation sites of control and *P1P2* cKO mice. β-actin serves as a loading control. (*E*) Quantification of the results shown in *D* ($n = 3$ per genotype and mean ± SEM). $^{*}P < 0.05$ and $^{**}P < 0.01$ (Student's *t* test).

Dio2 expression in GD 6 implantation sites of *P1P2* cKO mice (Fig. 6*B*).

To determine if the absence of PARP-1 and PARP-2 resulted in an increase of senescent cells, we quantified senescence-associated β-galactosidase (SA-βG) activity, an established marker of senescence (43) in GD 6 implantation sites. Quantitative analysis confirmed an increase in cellular senescence based on SA-βG activity in *P1P2* cKO mice (Fig. 6*C*). Additionally, we isolated uterine stromal cells on GD 4 and induced them to decidualize in vitro. The cells from *P1P2* cKO mice displayed a blunted decidual response and an increase in Sa-βG activity (Fig. 6 *D* and *E*). To further explore the connection between aberrant decidualization and senescence, we compared the expression of genes known to be involved in decidualization and senescence in control and *P1P2* cKO mice on GD 6. A significant percentage of genes present in both the decidualization and senescent gene lists were differentially expressed in the implantation sites of *P1P2* cKO mice on GD 6 (*SI Appendix*, Fig. S6*A* and Datasets S2 and S3). Taken together, these data suggest that the implantation sites of *P1P2* cKO mice on GD 6 have an increased population of senescent decidual cells.

The primary mechanism of cell cycle arrest triggered by p53 is the p21-mediated stabilization of the dimerization partner RB-like E2F and multivulval class B (DREAM) complex, a transcriptional repressor that binds to E2F and CHR promoter sites (44). Utilizing the Mining Algorithm for Genetic Controllers (MAGIC) (45), we found that E2F transcription factors were predicted to drive the transcriptomic differences observed

Downloaded at Palestinian Territory, occupied on December 21, 2021

www.manaraa.com

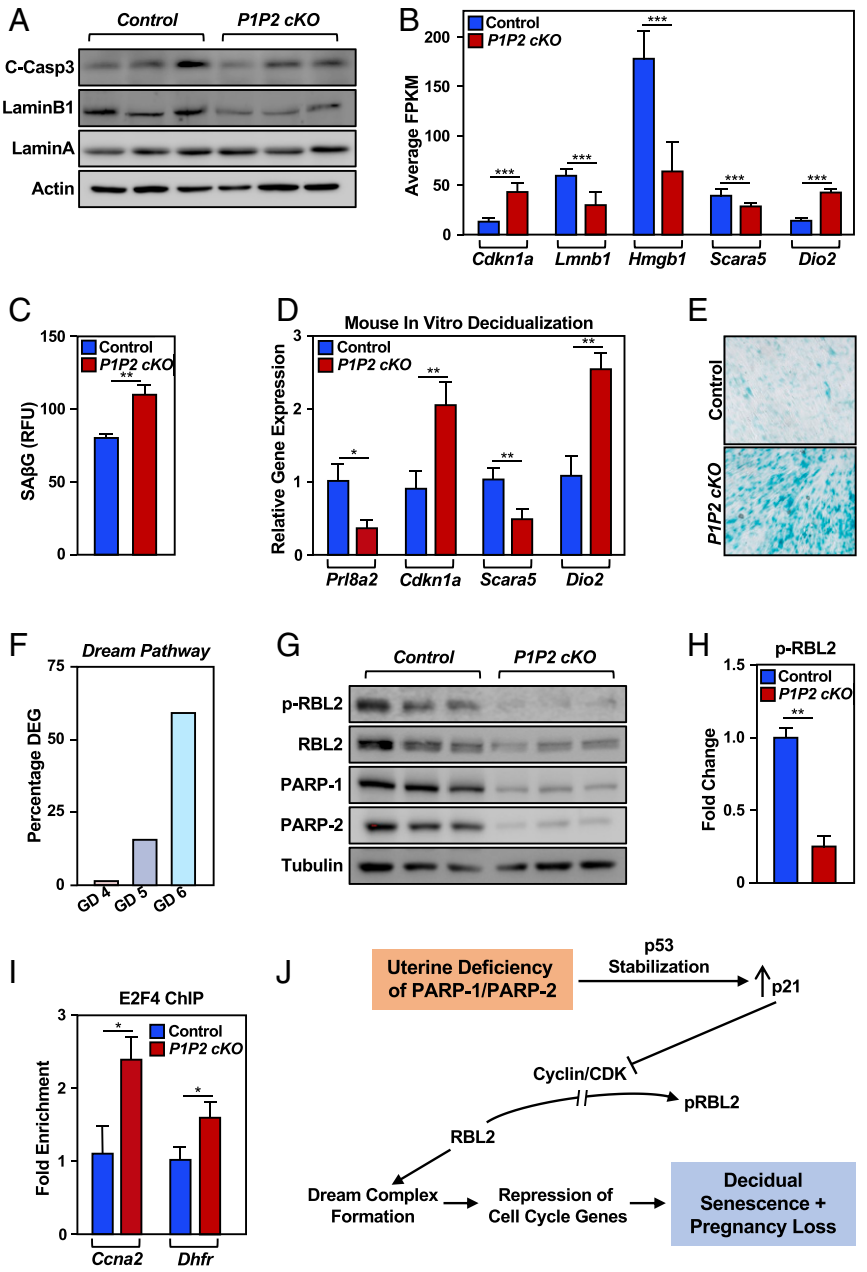

Fig. 6. PARP-1;PARP-2 deficiency results in cell cycle arrest and cellular senescence. (*A*) Western blot analysis of cleaved caspase-3 (C-Casp3), LMNB1, LMNA, and p-H2A.X in GD6 implantation sites of control and *P1P2* cKO mice. β-actin serves as a loading control. (*B*) Expression levels (Fragments per kilobase of exon per million mapped fragments, FPKM) from GD 6 RNA-seq data of established marker genes of cellular senescence and diverging senescence decidual cells in vivo. (*C*) SA-βG activity, expressed in relative fluorescence intensity units (RFU), in GD 6 implantation sites of control and *P1P2* cKO mice ($n = 3$ per genotype and mean ± SEM). $^{**}P < 0.01$ (Student's *t* test). (*D*) RT-PCR of mRNA from mouse primary endometrial stromal cells after 3 d of decidualization ($n = 3$ per genotype and mean ± SEM). $^{*}P < 0.05$ and $^{**}P < 0.01$ (Student's *t* test). (*E*) Representative SA-βG staining in mouse primary, endometrial stromal cells after 3 d of decidualization. (*F*) Bar graph of the percent of genes in the p53 DREAM pathway that are differentially expressed between control and *P1P2* cKO mice on GDs 4, 5, and 6. The hypergeometric *P* values of overrepresentation of p53 Dream pathway are $P = 0.85$ (GD 4), $P = 0.99$ (GD 5), and $^{****}P = 1.36 \times 10^{-30}$ (GD 6). (*G*) Western blot analysis of p-Rbl2, Rbl2, PARP-1, and PARP-2 in GD6 implantation sites of control and *P1P2* cKO mice. β-tubulin serves as a loading control. (*H*) Quantification of the results shown in *G* ($n = 3$ per genotype and mean ± SEM). $^{*}P < 0.05$ and $^{**}P < 0.01$ (Student's *t* test). (*I*) E2F4 enrichment was assessed by ChIP-qPCR at the *Ccna2* and *Dhfr* gene promoters in GD 6 implantation sites ($n = 3$ per genotype and mean ± SEM). $^{*}P < 0.05$ and $^{**}P < 0.01$ (Student's *t* test). (*J*) Potential pathway that promotes decidual senescence and pregnancy loss in *P1P2* cKO mice.

between the control and *P1P2* cKO mouse decidua and that E2F- and CHR-binding motifs were significantly enriched in differentially expressed decidualization-associated genes (*SI Appendix*, Fig. S7 *B* and *C*). The DREAM pathway coordinately down-regulates more than 250 genes implicated in DNA replication, mitotic spindle assembly, nucleosome packaging, and chromosome segregation (46). The comparison of expression of DREAM targets between control and *P1P2* cKO mice revealed no differences on GDs 4 and 5. In contrast, 55% of the genes regulated by the DREAM pathway were down-regulated in the *P1P2* cKO decidua (Fig. 6*F*). These results indicate that the DREAM complex is hyperactive during pregnancy in uteri-deficient PARP-1 and PARP-2.

The hyperactivation of the DREAM complex may be a consequence of p21 inhibition by CDK4. The phosphorylation of

Downloaded at Palestinian Territory, occupied on December 21, 2021

www.manaraa.com

retinoblastoma protein-like protein 2 (Rbl2) by CDK4 is required to weaken the activity of DREAM complex to allow the progression of the cell cycle (47). Western blot analysis of whole-cell extracts revealed that Rbl2 is hypophosphorylated in the decidua of *P1P2* cKO mice on GD 6 (Fig. 6 *G* and *H*). Finally, in chromatin immunoprecipitation (ChIP) assays, we observed an increase in E2F4 levels at the promotors of genes (*Ccna2* and *Dhfr*) found in the DREAM pathway and down-regulated in the *P1P2* cKO GD 6 uterus (Fig. 6*I*). Overall, these results provide evidence that increased DNA damage in the absence of PARP-1 and PARP-2 leads to the p53-mediated suppression of the cell cycle through the DREAM complex, cumulating in increased decidual cell senescence and pregnancy failure (Fig. 6*J*).

Discussion

We report a previously unrecognized role for PARP-1 and PARP-2 in regulating adult uterine function and fertility and provide evidence that they have essential roles in stromal cell decidualization and pregnancy success. Specifically, we observed that the chemical inhibition or uterine-specific genetic depletion of PARP-1 and PARP-2 results in severe subfertility. Although embryo attachment and the onset of stromal cell decidualization proceed in the absence of uterine PARP-1 and PARP-2, implantation site size was significantly reduced. Mechanistically, the decidualizing stromal cells of PARP-1– and PARP-2–deficient mice display increased DNA damage and p53 activation, which promotes cell cycle arrest and cellular senescence as a driver of the observed infertility or severe subfertility.

Roles for Nuclear PARPs and ADPRylation in Implantation Biology. Previous studies have shown that individual knockouts of *Parp1* or *Parp2* result in mice that are viable, whereas double knockout of *Parp1* and *Parp2* results in embryonic lethality at the onset of gastrulation (24, 25). Of note, female $Parp1^{\pm};Parp2^{-/-}$ mice are poorly fertile (25), suggesting a critical unexplored role in pregnancy biology. But the lack of viability in double null *Parp1* and *Parp2* mice precludes their use for the study of the potential, redundant roles of PARP-1 and PARP-2 in female reproductive biology. This led us to develop tissue-specific uterine double knockouts of PARP-1 and PARP-2, which we used to study the role of PARP-1 and PARP-2 in regulating stromal cell decidualization and pregnancy success. Our studies using this model have elucidated specific roles for PARP-1 and PARP-2 in distinct processes related to implantation.

In the mouse, the initiation of the attachment reaction occurs within implantation crypts on the AM side of the uterus (27, 48). Although implantation can occur on the mesometrial side of the uterus, it results in an increased incidence of embryo resorption and pregnancy loss (27, 49). We observed embryo attachment within the implantation crypts on the AM side of the uterus with the chemical inhibition or genetic depletion of PARP-1 and PARP-2. On-time blastocyst implantation is essential to trigger stromal cell decidualization, which is critical for pregnancy success in mice and humans, since it regulates placental development and the growth and development of the embryo (2, 29). Perturbations in the blastocyst positioning and timing of early pregnancy events can elicit adverse ripple effects and compromise pregnancy outcomes (2, 48, 49). Based on our RNA-seq analysis, *Hbegf*, one of the first established molecular mediators of blastocyst–uterine interactions, expression is unchanged in the *P1P2* cKO mouse uterus on GD 4 or 5 (50). In addition, only 103 genes were differentially expressed in the *P1P2* cKO uterus on GD 4, and genes critical for conferring uterine receptivity and embryo uterine communication (*Msx1*, *Msx2*, *Lif*, *Hbegf*, *Klf5 Wnt5a*, and *Vangl2*) are not altered (2, 27, 48, 49, 51, 52). Thus, the presence and activity of PARP-1 and PARP-2 are not essential for uterine receptivity, embryo transport, localization, or attachment during early pregnancy.

The induced expression of PTGS2 at the site of blastocyst attachment further suggests unperturbed epithelial–mesenchymal interactions during the attachment reaction. PTGS2 is a marker of stromal cell decidualization and is important for the onset of decidualization (28, 50). Although we observed comparable levels and the localization of PTGS2 within the implantation chamber of control and *P1P2* uterine cKO mice on GDs 5 and 6, there was a decrease in implantation site size on GDs 6 and 8. In this regard, the uteri of *P1P2* cKO exhibited an attenuated decidual response using an artificial model of decidualization. Together, these results indicate that the attachment reaction has occurred, and decidualization is correctly initiated at GD 5 in *P1P2* cKO mice but that decidualization fails to progress properly or is prematurely arrested.

Increased Senescence at Implantation Sites in the Absence of PARP-1 and PARP-2. The decidualization defects observed in the physiological studies were also reflected in the transcriptome analysis. We observed a large perturbation in the transcriptome of GD 6 implantation sites of *P1P2* cKO mice compared to control mice. Of note, the expression of numerous genes involved in the decidual response was significantly altered. GO analysis highlighted an increase in p53-mediated signal transduction and decreased cell cycle progression. The importance of signaling transduction by p53 and processes involved in cell cycle progression throughout decidualization has been well studied (6, 7, 53). Previous studies have linked p53 function to pregnancy success and implantation phenotypes, but the results from null and cKO animals have often been inconsistent (31).

Several recent studies using a model of human stromal cell decidualization and endometrial biopsies have demonstrated that cell cycle arrest and decidual senescence is implicated in recurrent early pregnancy loss, since chronic senescence is incompatible with the formation of a functional decidua (42, 54). In fact, the endometrium of women with recurrent pregnancy loss is characterized by heightened cellular senescence and a prolonged decidual inflammatory response (55, 56). Our gene expression analysis and the observed increase in SA-βG activity indicated a heightened level of senescent decidual cells in *P1P2* cKO mouse implantation sites on GD 6.

Increased p53 Signal Transduction and Hyperactivation of the DREAM Pathway in Implantation Sites in the Absence of PARP-1 and PARP-2. Uterine decidualization is characterized by extensive proliferation, differentiation, and endoreduplication (6, 29). Increased DNA damage has been reported within implantation sites, compared to interimplantation sites during early mouse gestation, and polyploidization can be induced by persistent DNA damage signaling (32, 57). In the present study, we observed increased DNA damage, but no corresponding increase in apoptotic cells, in the decidua of GD 6 *P1P2* cKO mice compared to control mice. Cell cycle arrest and, ultimately, cellular senescence can result from the inability to induce apoptosis in conditions of persistent DNA damage (41). The primary mechanism for G2/M cell cycle arrest is triggered by the p53 up-regulation of p21 and the subsequent stabilization of the transcription repressor DREAM complex (44). Our observation of increased p53 phosphorylation and *Cdkn1a* expression coupled to the enriched repression of the DREAM pathway in the decidua of P1P2 cKO mice is indicative of the inability of mouse stromal cells to induce apoptosis in response to DNA damage in the absence or PARP-1 and PARP-2.

Posttranslational modifications of p53 control its function (33). For example, the phosphorylation of serine 15 on p53 is a focal point in the activation and stabilization of p53 (58). Moreover, the ADPRylation of p53 inhibits its interactions with DNA elements across the genome and, thus, represents a means of regulating p53-dependent transcriptional activation (36, 59–62). ADPRylation sites are enriched near the phosphorylation sites across the human proteome (22, 37, 38), and ADPRylation and phosphorylation of

PHYSIOLOGY

Downloaded at Palestinian Territory, occupied on December 21, 2021

www.manaraa.com

the same or nearby residues may be functionally antagonistic (22, 38, 63). Using bioinformatic analyses, we found that the top predicted sites of ADPRylation on p53 occur adjacent to serine 15 (Ser-15). Interestingly, we did not observe an increase in *Trp53* mRNA levels (RNA-seq data) but did observe an increase in p53 protein levels. This inconsistency indicates that the increase in the levels of p53 protein was not due to the overexpression of *Trp53* but rather the suppression of p53 protein degradation. The phosphorylation of p53 at Ser-15, as observed in our study, can inhibit the binding of the p53-degrading enzyme Mdm2, resulting in the stabilization of p53 (64). Furthermore, PARP inhibitor treatment was found to increase the phosphorylation of p53 at Ser-15 in neural progenitor cells and inhibit the binding of Mdm2 and p53 degradation (59). Thus, the reduced ADPRylation of p53 in the absence of PARP-1 and PARP-2 may result in increased phosphorylation, p53 stabilization, and cellular senescence.

Summary and Perspectives. In summary, using a combination of mouse genetic models, pharmacological inhibitors, and histological and transcriptomic analysis, we have identified roles for PARPs and ADPRylation during the establishment and maintenance of pregnancy. Our data suggest that PARP-1 and PARP-2 augment the DNA damage response in the developing decidua, presumably by ADPRylating substrate proteins, such as p53. Ultimately, the absence of PARP-1 and PARP-2 leads to increased decidual cell senescence and pregnancy failure. Further experimentation is necessary to thoroughly interrogate the substrate proteins of PARP-1 and PARP-2 in the developing decidua. Such information will provide a more thorough understanding of the biological functions of PARP-1 and PARP-2 in physiological systems. Potential translational outcomes may result in the development of contraceptive strategies and treatments for female reproductive disorders using FDA-approved PARP inhibitors. Furthermore, our findings raise the possibility of using the level of ADPRylation as a biomarker of uterine receptivity and stromal cell decidualization.

Materials and Methods

Additional descriptions of the Materials and Methods can be found in *SI Appendix*.

Use of Animals. All animal procedures were approved by the Institutional Animal Care and Use Committee of the University of Texas Southwestern Medical Center and were conducted according to NIH Guide for the Care and Use of Laboratory Animals (65). *Parp1*$^{f/f}$ mice were generated in the Kraus Laboratory from the European Conditional Mouse Mutagenesis Program stock (66) and are available from the Jackson Laboratory (stock No. 032650). *Parp2*$^{f/f}$ mice have been described previously (67). Individual floxed *Parp1* and *Parp2* lines were crossed to produce *Parp*$^{f/f}$;*Parp2*$^{f/f}$, and those mice were crossed with *Pgr*-Cre mice to generate cKO uterine animals. *Pgr*-Cre mice have been described previously (26). Gestational time points were obtained by the mating of 8- to 10-wk-old females *Parp1*$^{f/f}$;*Parp2*$^{f/f}$ (control) or *Pgr*$^{Cre/+}$ *Parp2*$^{f/f}$;*Parp2*$^{f/f}$ cKO females (*P1P2* cKO) with wild-type male mice. For all experiments, the day of vaginal plug observation was considered GD 1.

Visualization of Implantation Sites. GD 5 and GD 6 implantation sites were visualized by intravenous injection of 1% Evans blue dye (Sigma-Aldrich) before necropsy. Implantation sites and interimplantation sites were dissected and then frozen in liquid nitrogen or fixed with 4% paraformaldehyde. To confirm pregnancy in plug-positive females with no visual implantation sites, uterine horns were flushed and examined for the presence of blastocysts.

Fertility Analysis. For the fertility studies, individual adult female control and *P1P2* cKO mice were placed with a C57BL/6 male mouse of proven fertility for 6 mo, and the number of litters and pups born during that period were recorded.

Chemical Inhibition of PARP-1 and PARP-1. Wild-type mice were given intraperitoneal injections of Nir (25 mg/kg; Selleck Chemicals, S7625) or vehicle at 0900 h on GD 3 and GD 4. Control and Nir-treated mice were then housed separately until implantation analysis.

Artificial Decidualization. The induction of artificial decidual responses has been described previously (68).

Isolation and Culture of Uterine Stromal Cells. Mouse uterine stromal cells were isolated on GD 4, as described previously (48, 69). After an initial plating for 1 h at 37 °C, the unattached epithelial cells were removed, and the medium was replaced with fresh Dulbecco's Modified Eagle Medium/F12 containing 2% charcoal-stripped fetal bovine serum. The following day, in vitro decidualization was induced by treating endometrial stromal cells with 10 nM E2 and 1 μM P4. Stromal cells were decidualized for 72 h prior to analysis.

Antibodies. A detailed list of antibodies is provided in *SI Appendix*.

Immunofluorescent and Immunohistochemical Staining. At least three implantation sites were examined per mouse, GD timepoint, and genotype. Uteri were fixed in 4% paraformaldehyde in phosphate-buffered saline (PBS) overnight, dehydrated in ethanol, embedded in paraffin wax, and sectioned (5 μm). Sections were mounted on slides, deparaffinized in xylene, and rehydrated in a graded alcohol series. Deparaffinized sections were subjected to antigen retrieval by incubating sections in boiling 10 mM citrate buffer (pH 6.0) for 10 min, followed by cooling to room temperature. For peroxidase-based staining, sections were incubated with 5% H_2O_2 for 10 min. The slides were blocked and incubated with primary antibodies overnight at 4 °C in 1% bovine serum albumin (BSA) in PBS. The slides were washed and incubated with 5 μg/mL biotinylated secondary goat antibody. Immunohistochemical staining was visualized using Vectastain avidin–biotin complex kit (Catalog No. PK-6101, Vector Laboratories) and diaminobenzidine tetrahydrochloride as the chromagen. Sections were lightly counterstained with hematoxylin before affixing coverslips with Permount. Immunofluorescence visualization was performed with Alexa 488– or Alexa 594–conjugated secondary antibodies. Sections were counterstained with Hoechst 33342 (2 μg/mL; Thermo Fisher Scientific, PI62249). The quantification of stained slides was performed by ImageJ using three independent biological replicates, as previously described (70).

Preparation of Whole-Cell Lysates. Uterine tissue (GD 4) or implantation sites (following embryo removal) were reduced to a fine powder under liquid N2 using a tissue pulverizer and lysed with cell lysis buffer (20 mM Tris·HCl pH 7.5, 150 mM NaCl, 1 mM EDTA, 1 mM EGTA, 1% Nonidet P-40, 1% sodium deoxycholate, and 0.1% SDS) containing the following: 250 nM ADP-HPD (Aldrich-Sigma, A0627; a PARG inhibitor to prevent PAR chain cleavage during extraction), 20 μM PJ34 (a PARP inhibitor to prevent PAR synthesis during extraction), 1× phosphatase inhibitor mixture (Sigma-Aldrich, P0044 and P5726), and 1× complete protease inhibitor mixture (Roche, 11697498001). The lysates were incubated on ice for 30 min with gentle mixing and clarified by centrifugation at 21,000 RCF in a microfuge for 15 min at 4 °C.

Determination of Protein Concentrations and Western Blotting. Protein concentrations in the lysates were determined using Bradford reagent (Bio-Rad, 50000006). The lysates were run on 8 or 12% polyacrylamide-SDS gels and transferred to a nitrocellulose membrane. Blocked membranes were incubated with primary antibodies in 1% nonfat milk made in Tris-buffered saline containing 0.1% Tween 20 (TBST) or 2.5% BSA (for phosphorylation blots) overnight at 4 °C, followed by anti-rabbit HRP-conjugated IgG (1:5,000) or anti-mouse HRP-conjugated IgG (1:5,000) for 1 h at room temperature. Western blot signals were detected using an enhanced chemiluminescence detection reagent (Thermo Fisher Scientific, 34077 and 34095).

Quantification of SA-βG Activity. SA-βG in whole-tissue lysates was quantified using the 96-well cellular senescence activity assay kit (Cell Biolabs Inc, CBA-231), according to manufactures instructions.

Immunoprecipitation. Aliquots of tissue extract containing 1 mg total protein were used for immunoprecipitation. The extracts were precleared with IgG for 30 min, followed by incubation with Pierce protein A/G magnetic beads (Thermo Fisher Scientific, PI88802) for 30 min at 4 °C. The precleared extract was mixed with anti-p53 mouse monoclonal antibody and Pierce protein A/G magnetic beads overnight at 4 °C. The next day, the beads were washed three times with wash buffer (20 mM Hepes pH 7.9, 400 mM NaCl, 1.5 mM $MgCl_2$, 0.2 mM EDTA, 1% Nonidet P-40, 1 mM DTT, 1× protease inhibitor mixture, 250 nM APD-HPD, and 20 μM PJ34). The beads were collected and mixed with 1.5× SDS-PAGE loading buffer, followed by incubation at 100 °C for 10 min. The samples were analyzed by Western blotting.

Downloaded at Palestinian Territory, occupied on December 21, 2021
www.manaraa.com

RNA Isolation and RT-qPCR. Samples were collected at the indicated time points and total RNA was isolated using RNeasy kit (Qiagen), according to the manufacturer's instructions. Total RNA was reverse transcribed using oligo(dT) primers and Moloney Murine Leukemia Virus reverse transcriptase (Promega) to generate complementary DNA (cDNA). The cDNA samples were subjected to qPCR using the gene-specific primers listed in *SI Appendix*.

RNA-Seq. RNA-seq libraries were prepared, evaluated, sequenced, and analyzed as follows.

RNA isolation. We used two biological replicates of pooled uteri or implantation sites from independent collections for each GD. Biological replicates were generated by pooling total RNA from three mice (3 to 4 implantation sites per mouse). RNA was isolated using RNeasy kit (Qiagen), according to the manufacturer's instructions. The total RNA was enriched for polyA+ RNA using Dynabeads Oligo(dT)25 (Invitrogen, 61002). The polyA+ RNA was used to generate strand-specific RNA-seq libraries, as described previously (71). The RNA-seq libraries were subjected to quality control (QC) analyses and sequenced using an Illumina HiSEq. 2500.

Quality assessment, differential expression analysis, and data visualization. The data were assessed, analyzed, and visualized as described previously (21, 66). The prediction of putative transcription factors driving gene expression changes was performed using MAGIC: A tool for predicting transcription factors and cofactors driving gene sets using Encyclopedia of DNA Elements (ENCODE) data (45).

ChIP-qPCR. Implantation sites (following embryo removal) were reduced to a fine powder under liquid N2 using a tissue pulverizer and fixed with 1% formaldehyde in PBS for 15 min. Fixation was quenched by the addition of 125 mM. The fixed tissue was subjected to ChIP as described previously (21, 38). The ChIPed genomic DNA was subjected to qPCR using the gene-specific primers listed in *SI Appendix*.

Bioinformatic Prediction of ADPRylated Residues of on Mouse p53. The prediction of ADPRylation sites for p53 (UniProt entry: P02340) was performed using the online tool ADPredict (39).

Statistical Analyses. All Western blots with quantification were performed with a minimum of three independent biological replicates and analyzed by ImageJ. The data are presented as the mean ± SEM, as determined from at least three independent experiments. Following the Shapiro–Wilk test for normality, the data were analyzed using Student's *t* test. A *P* value of less than 0.05 was considered statistically significant. Statistical analyses for the genomic experiments were performed using standard genomic statistical tests, as described in the *SI Appendix*.

Data Availability. RNA-seq datasets have been deposited in the National Center for Biotechnology Information's Gene Expression Omnibus repository (GSE169544) (72). All other study data are included in the article and/or supporting information.

ACKNOWLEDGMENTS. We thank the members of the W.L.K. laboratory for input and feedback on this project and comments on this manuscript; the University of Texas (UT) Southwestern Next-Generation Sequencing Core under the direction of Ralf Kittler; and the UT Southwestern Histo Pathology Core. This work was supported by NIH, National Institute of Diabetes, Digestive, and Kidney Disorders (NIDDK) Grant R01 DK069710, NIH, National Institute of Child Health and Human Development (NICHD) Grant P01 HD087150, funds from the Cecil H. and Ida Green Center for Reproductive Biology Sciences Endowment to W.L.K., and NIH/NICHD Postdoctoral Fellowship F32 HD100103 to A.M.K.

1. R. Rai, L. Regan, Recurrent miscarriage. *Lancet* **368**, 601–611 (2006).
2. J. Cha, X. Sun, S. K. Dey, Mechanisms of implantation: Strategies for successful pregnancy. *Nat. Med.* **18**, 1754–1767 (2012).
3. H. Carp *et al.*, Karyotype of the abortus in recurrent miscarriage. *Fertil. Steril.* **75**, 678–682 (2001).
4. M. Ogasawara, K. Aoki, S. Okada, K. Suzumori, Embryonic karyotype of abortuses in relation to the number of previous miscarriages. *Fertil. Steril.* **73**, 300–304 (2000).
5. B. Gellersen, I. A. Brosens, J. J. Brosens, Decidualization of the human endometrium: Mechanisms, functions, and clinical perspectives. *Semin. Reprod. Med.* **25**, 445–453 (2007).
6. S. K. Das, Regional development of uterine decidualization: Molecular signaling by Hoxa-10. *Mol. Reprod. Dev.* **77**, 387–396 (2010).
7. J. Tan *et al.*, Evidence for coordinated interaction of cyclin D3 with p21 and cdk6 in directing the development of uterine stromal cell decidualization and polyploidy during implantation. *Mech. Dev.* **111**, 99–113 (2002).
8. J. Yuan *et al.*, Tridimensional visualization reveals direct communication between the embryo and glands critical for implantation. *Nat. Commun.* **9**, 603 (2018).
9. A. M. Kelleher, J. Milano-Foster, S. K. Behura, T. E. Spencer, Uterine glands coordinate on-time embryo implantation and impact endometrial decidualization for pregnancy success. *Nat. Commun.* **9**, 2435 (2018).
10. T. Garrido-Gomez *et al.*, Defective decidualization during and after severe preeclampsia reveals a possible maternal contribution to the etiology. *Proc. Natl. Acad. Sci. U.S.A.* **114**, E8468–E8477 (2017).
11. B. A. Gibson, W. L. Kraus, New insights into the molecular and cellular functions of poly(ADP-ribose) and PARPs. *Nat. Rev. Mol. Cell Biol.* **13**, 411–424 (2012).
12. V. Schreiber, F. Dantzer, J.-C. Ame, G. de Murcia, Poly(ADP-ribose): Novel functions for an old molecule. *Nat. Rev. Mol. Cell Biol.* **7**, 517–528 (2006).
13. R. Gupte, Z. Liu, W. L. Kraus, PARPs and ADP-ribosylation: Recent advances linking molecular functions to biological outcomes. *Genes Dev.* **31**, 101–126 (2017).
14. R. Krishnakumar *et al.*, Reciprocal binding of PARP-1 and histone H1 at promoters specifies transcriptional outcomes. *Science* **319**, 819–821 (2008).
15. Z. Liu, W. L. Kraus, Catalytic-independent functions of PARP-1 determine Sox2 pioneer activity at intractable genomic loci. *Mol. Cell* **65**, 589–603.e9 (2017).
16. N. Nalabothula *et al.*, Genome-wide profiling of PARP1 reveals an interplay with gene regulatory regions and DNA methylation. *PLoS One* **10**, e0135410 (2015).
17. P. Bai *et al.*, PARP-2 regulates SIRT1 expression and whole-body energy expenditure. *Cell Metab.* **13**, 450–460 (2011).
18. M. O. Hottiger, Nuclear ADP-ribosylation and its role in chromatin plasticity, cell differentiation, and epigenetics. *Annu. Rev. Biochem.* **84**, 227–263 (2015).
19. R. Krishnakumar, W. L. Kraus, The PARP side of the nucleus: Molecular actions, physiological outcomes, and clinical targets. *Mol. Cell* **39**, 8–24 (2010).
20. F. Zhang *et al.*, Poly(ADP-ribose) polymerase 1 is a key regulator of estrogen receptor α-dependent gene transcription. *J. Biol. Chem.* **288**, 11348–11357 (2013).
21. X. Luo *et al.*, PARP-1 controls the adipogenic transcriptional program by PARylating C/EBPβ and modulating its transcriptional activity. *Mol. Cell* **65**, 260–271 (2017).
22. B. A. Gibson *et al.*, Chemical genetic discovery of PARP targets reveals a role for PARP-1 in transcription elongation. *Science* **353**, 45–50 (2016).
23. D.-S. Kim *et al.*, Activation of PARP-1 by snoRNAs controls ribosome biogenesis and cell growth via the RNA helicase DDX21. *Mol. Cell* **75**, 1270–1285.e14 (2019).
24. J. M. de Murcia *et al.*, Requirement of poly(ADP-ribose) polymerase in recovery from DNA damage in mice and in cells. *Proc. Natl. Acad. Sci. U.S.A.* **94**, 7303–7307 (1997).
25. J. Ménissier de Murcia *et al.*, Functional interaction between PARP-1 and PARP-2 in chromosome stability and embryonic development in mouse. *EMBO J.* **22**, 2255–2263 (2003).
26. S. M. Soyal *et al.*, Cre-mediated recombination in cell lineages that express the progesterone receptor. *Genesis* **41**, 58–66 (2005).
27. J. Cha *et al.*, Appropriate crypt formation in the uterus for embryo homing and implantation requires Wnt5a-ROR signaling. *Cell Rep.* **8**, 382–392 (2014).
28. H. Lim *et al.*, Multiple female reproductive failures in cyclooxygenase 2-deficient mice. *Cell* **91**, 197–208 (1997).
29. B. Gellersen, J. J. Brosens, Cyclic decidualization of the human endometrium in reproductive health and failure. *Endocr. Rev.* **35**, 851–905 (2014).
30. W. Deng *et al.*, p53 coordinates decidual sestrin 2/AMPK/mTORC1 signaling to govern parturition timing. *J. Clin. Invest.* **126**, 2941–2954 (2016).
31. Y. Hirota *et al.*, Uterine-specific p53 deficiency confers premature uterine senescence and promotes preterm birth in mice. *J. Clin. Invest.* **120**, 803–815 (2010).
32. W. Lei *et al.*, Progesterone and DNA damage encourage uterine cell proliferation and decidualization through up-regulating ribonucleotide reductase 2 expression during early pregnancy in mice. *J. Biol. Chem.* **287**, 15174–15192 (2012).
33. B. Gu, W.-G. Zhu, Surf the post-translational modification network of p53 regulation. *Int. J. Biol. Sci.* **8**, 672–684 (2012).
34. J. A. Muñoz-Gámez *et al.*, PARP inhibition sensitizes p53-deficient breast cancer cells to doxorubicin-induced apoptosis. *Biochem. J.* **386**, 119–125 (2005).
35. C. Conde *et al.*, Loss of poly(ADP-ribose) polymerase-1 causes increased tumour latency in p53-deficient mice. *EMBO J.* **20**, 3535–3543 (2001).
36. M. Malanga, J. M. Pleschke, H. E. Kleczkowska, F. R. Althaus, Poly(ADP-ribose) binds to specific domains of p53 and alters its DNA binding functions. *J. Biol. Chem.* **273**, 11839–11843 (1998).
37. S. C. Larsen, I. A. Hendriks, D. Lyon, L. J. Jensen, M. L. Nielsen, Systems-wide analysis of serine ADP-ribosylation reveals widespread occurrence and site-specific overlap with phosphorylation. *Cell Rep.* **24**, 2493–2505.e4 (2018).
38. D. Huang *et al.*, Functional interplay between histone H2B ADP-ribosylation and phosphorylation controls adipogenesis. *Mol. Cell* **79**, 934–949.e14 (2020).
39. M. Lo Monte, C. Manelfi, M. Gemei, D. Corda, A. R. Beccari, ADPredict: ADP-ribosylation site prediction based on physicochemical and structural descriptors. *Bioinformatics* **34**, 2566–2574 (2018).
40. B. G. Childs, D. J. Baker, J. L. Kirkland, J. Campisi, J. M. van Deursen, Senescence and apoptosis: Dueling or complementary cell fates? *EMBO Rep.* **15**, 1139–1153 (2014).
41. Y. Qian, X. Chen, Tumor suppression by p53: Making cells senescent. *Histol. Histopathol.* **25**, 515–526 (2010).
42. E. S. Lucas *et al.*, Recurrent pregnancy loss is associated with a pro-senescent decidual response during the peri-implantation window. *Commun. Biol.* **3**, 37 (2020).
43. F. Debacq-Chainiaux, J. D. Erusalimsky, J. Campisi, O. Toussaint, Protocols to detect senescence-associated beta-galactosidase (SA-betagal) activity, a biomarker of senescent cells in culture and in vivo. *Nat. Protoc.* **4**, 1798–1806 (2009).
44. M. Quaas, G. A. Müller, K. Engeland, p53 can repress transcription of cell cycle genes through a p21(WAF1/CIP1)-dependent switch from MMB to DREAM protein complex binding at CHR promoter elements. *Cell Cycle* **11**, 4661–4672 (2012).

Downloaded at Palestinian Territory, occupied on December 21, 2021

www.manaraa.com

45. A. Roopra, MAGIC: A tool for predicting transcription factors and cofactors driving gene sets using ENCODE data. *PLoS Comput. Biol.* **16**, e1007800 (2020).
46. K. Engeland, Cell cycle arrest through indirect transcriptional repression by p53: I have a DREAM. *Cell Death Differ.* **25**, 114–132 (2018).
47. K. Z. Guiley *et al*., Structural mechanisms of DREAM complex assembly and regulation. *Genes Dev.* **29**, 961–974 (2015).
48. T. Daikoku *et al*., Conditional deletion of Msx homeobox genes in the uterus inhibits blastocyst implantation by altering uterine receptivity. *Dev. Cell* **21**, 1014–1025 (2011).
49. J. Yuan *et al*., Planar cell polarity signaling in the uterus directs appropriate positioning of the crypt for embryo implantation. *Proc. Natl. Acad. Sci. U.S.A.* **113**, E8079–E8088 (2016).
50. S. K. Das *et al*., Heparin-binding EGF-like growth factor gene is induced in the mouse uterus temporally by the blastocyst solely at the site of its apposition: A possible ligand for interaction with blastocyst EGF-receptor in implantation. *Development* **120**, 1071–1083 (1994).
51. X. Sun *et al*., Kruppel-like factor 5 (KLF5) is critical for conferring uterine receptivity to implantation. *Proc. Natl. Acad. Sci. U.S.A.* **109**, 1145–1150 (2012).
52. C. L. Stewart *et al*., Blastocyst implantation depends on maternal expression of leukaemia inhibitory factor. *Nature* **359**, 76–79 (1992).
53. S. K. Das, Cell cycle regulatory control for uterine stromal cell decidualization in implantation. *Reproduction* **137**, 889–899 (2009).
54. P. J. Brighton *et al*., Clearance of senescent decidual cells by uterine natural killer cells in cycling human endometrium. *eLife* **6**, e31274 (2017).
55. E. S. Lucas *et al*., Loss of endometrial plasticity in recurrent pregnancy loss. *Stem Cells* **34**, 346–356 (2016).
56. M. S. Salker *et al*., Disordered IL-33/ST2 activation in decidualizing stromal cells prolongs uterine receptivity in women with recurrent pregnancy loss. *PLoS One* **7**, e52252 (2012).
57. T. Davoli, E. L. Denchi, T. de Lange, Persistent telomere damage induces bypass of mitosis and tetraploidy. *Cell* **141**, 81–93 (2010).
58. J. Loughery, M. Cox, L. M. Smith, D. W. Meek, Critical role for p53-serine 15 phosphorylation in stimulating transactivation at p53-responsive promoters. *Nucleic Acids Res.* **42**, 7666–7680 (2014).
59. A. Okuda *et al*., Poly(ADP-ribose) polymerase inhibitors activate the p53 signaling pathway in neural stem/progenitor cells. *BMC Neurosci.* **18**, 14 (2017).
60. C. A. Vivelo, R. Wat, C. Agrawal, H. Y. Tee, A. K. L. Leung, ADPriboDB: The database of ADP-ribosylated proteins. *Nucleic Acids Res.* **45**, D204–D209 (2017). Correction in: *Nucleic Acids Res.* **45**, 6254 (2017).
61. M.-H. Lee, H. Na, E.-J. Kim, H.-W. Lee, M.-O. Lee, Poly(ADP-ribosyl)ation of p53 induces gene-specific transcriptional repression of MTA1. *Oncogene* **31**, 5099–5107 (2012).
62. C. M. Simbulan-Rosenthal *et al*., Poly(ADP-ribosyl)ation of p53 in vitro and in vivo modulates binding to its DNA consensus sequence. *Neoplasia* **3**, 179–188 (2001).
63. E. Bartlett *et al*., Interplay of histone marks with serine ADP-ribosylation. *Cell Rep.* **24**, 3488–3502.e5 (2018).
64. E. Appella, C. W. Anderson, Post-translational modifications and activation of p53 by genotoxic stresses. *Eur. J. Biochem.* **268**, 2764–2772 (2001).
65. National Research Council, *Guide for the Care and Use of Laboratory Animals* (National Academies Press, Washington, DC, ed. 8, 2011).
66. K. W. Ryu *et al*., Metabolic regulation of transcription through compartmentalized NAD^+ biosynthesis. *Science* **360**, eaan5780 (2018).
67. J. Navarro *et al*., PARP-1/PARP-2 double deficiency in mouse T cells results in faulty immune responses and T lymphomas. *Sci. Rep.* **7**, 41962 (2017).
68. C. A. Finn, L. Martin, Endocrine control of the timing of endometrial sensitivity to a decidual stimulus. *Biol. Reprod.* **7**, 82–86 (1972).
69. T. Daikoku *et al*., Proteomic analysis identifies immunophilin FK506 binding protein 4 (FKBP52) as a downstream target of Hoxa10 in the periimplantation mouse uterus. *Mol. Endocrinol.* **19**, 683–697 (2005).
70. A. R. Crowe, W. Yue, Semi-quantitative determination of protein expression using immunohistochemistry staining and analysis: An integrated protocol. *Bio Protoc.* **9**, e3465 (2019).
71. S. Zhong *et al*., High-throughput illumina strand-specific RNA sequencing library preparation. *Cold Spring Harb. Protoc.* **2011**, 940–949 (2011).
72. A. Kelleher, R. Setlem, W. L. Kraus, PARP-1/PARP-2 double deficiency results in recurrent early pregnancy loss and decidualization failure in mice. NCBI GEO. https://www.ncbi.nlm.nih.gov/geo/query/acc.cgi?acc=GSE169544. Deposited 24 March 2021.

Downloaded at Palestinian Territory, occupied on December 21, 2021

www.manaraa.com